frontiers | Frontiers in Energy Research RETRACTED ON 18 SEPTEMBER 2025

TYPE Original Research
PUBLISHED 06 October 2022
DOI 10.3389/fenrg.2022.980042

OPEN ACCESS

EDITED BY
Adnan,
Mohi-ud-Din Islamic University, Pakistan

REVIEWED BY
Saqib Murtaza,
King Mongkut's University of Technology Thonburi, Thailand
Muhammad Bilal,
City University of Science and Information Technology, Pakistan
Muhammad Mubashir Bhatti,
Shandong University of Science and Technology, China

*CORRESPONDENCE
M. Riaz Khan,
mrkhan.math@gmail.com
Aatif Ali,
atifkh98@gmail.com

SPECIALTY SECTION
This article was submitted to Process and Energy Systems Engineering, a section of the journal Frontiers in Energy Research

RECEIVED 28 June 2022
ACCEPTED 09 August 2022
PUBLISHED 06 October 2022
RETRACTED 18 September 2025

CITATION
Khan MR, Ahammad NA, Alhazmi SE, Ali A, Abdelmohimen MAH, Allogmany R, Tag-Eldin E and Yassen MF (2022), Energy and mass transport through hybrid nanofluid flow passing over an extended cylinder with the magnetic dipole using a computational approach.
Front. Energy Res. 10:980042.
doi: 10.3389/fenrg.2022.980042

RETRACTED: Energy and mass transport through hybrid nanofluid flow passing over an extended cylinder with the magnetic dipole using a computational approach

M. Riaz Khan[1]*, N. Ameer Ahammad[2], Sharifah E. Alhazmi[3], Aatif Ali[4]*, Mostafa A. H. Abdelmohimen[5,6], Reem Allogmany[7], Elsayed Tag-Eldin[8] and Mansour F. Yassen[9,10]

[1]Department of Mathematics, Quaid-i-Azam University, Islamabad, Pakistan, [2]Department of Mathematics, Faculty of Science, University of Tabuk, Tabuk, Saudi Arabia, [3]Mathematics Department, Al-Qunfudah University College, Umm Al-Qura University, Mecca, Saudi Arabia, [4]Department of Mathematics, Abdul Wali Khan University Mardan, Mardan, Pakistan, [5]Mechanical Engineering Department, College of Engineering, King Khalid University, Abha, Saudi Arabia, [6]Shoubra Faculty of Engineering, Benha University, Cairo, Egypt, [7]Department of Mathematics, Faculty of Science, Taibah University, Al-Madinah Al-Munawwarah, Saudi Arabia, [8]Faculty of Engineering and Technology, Future University in Egypt, New Cairo, Egypt, [9]Department of Mathematics, College of Science and Humanities in Al-Aflaj, Prince Sattam Bin Abdulaziz University, Al-Kharj, Saudi Arabia, [10]Department of Mathematics, Faculty of Science, Damietta University, Damietta, Egypt

The objective of this research is to evaluate the heat and mass transfer in a water-based Darcy–Forchheimer hybrid nanofluid (HNF) flow across an expanding cylinder. The fluid flow has been studied under the influence of a magnetic field, viscous dissipation, heat source, thermal radiation, concentration stratification, and chemical reaction. Carbon nanotubes (CNTs) and iron ferrite (Fe_3O_4) nanoparticles (NPs) are added to the water, for the purpose of synthesizing the HNF. The fluid flow has been induced in the presence of gyrotactic microorganisms and the non-Fick's model. Microorganisms are used to stabilize scattered nanoparticles through the hybrid nanofluid. The phenomena have been modeled in the form of a nonlinear system of partial differential equations (PDEs). The modeled equations are reduced to a dimensionless system of ODEs by using similarity substitution. The numerical solution of the derived sets of nonlinear differential equations is obtained by using the parametric continuation method. The impact of physical constraints on temperature, velocity, concentration, and microorganism profiles is presented through figures and tables. It has been observed that the heat and mass transport rates increase with the rising effect of the curvature parameter, while declining with the effect of the thermal stratification parameter.

KEYWORDS

hybrid nanofluid, iron oxide, magnetic dipole, CNTs, PCM, gyrotactic microorganism, extended cylinder

Introduction

The study of boundary layer flow through a cylinder gained the attention of researchers due to its broad array of applications in numerous sectors, including manufacture and extraction of glass fiber, bridges and funnel stacks in civil engineering, paper production, melt-spinning rubber sheets, blood transportation in heart-lung machine, risers and channels, polymer production, carriage of noxious fluids at nuclear power plants, carriage of destructive fluids when fluid contact with machinery and equipment is restricted, and many others (Ma et al., 2020; Dou, 2022; Hussain et al., 2022). For about the last 2 decades, various investigators chose to conduct their research in the cylindrical channel because of the aforementioned applicability. The mathematical analysis of power-law nanofluid flow across a circular surface is documented by Ullah et al. (2021a) who concluded that the natural frequency has a momentous effect on the fluid's properties. Zhang et al. (2021) numerically assessed the HNF flow across a circular cylinder. It was observed that the rotating cylinders containing a splitting sheet, may be effective options for energy transfer. Numerical simulations and tests to lower the drag of a cylinder for both smooth and round cylinders with dimpled surfaces are investigated by Ullah et al. (2021b). The results show that within a particular range of Reynolds numbers, the dimpled structure can efficiently reduce cylinder drag, with a maximum drag reduction rate of up to 19%. Using the modified Fourier heat flux law, Varun Kumar et al. (2021) scrutinized the upshot of hybrid NPs on the dusty flow behavior through an enlarging cylinder. Their observations show that increasing particle mass concentration reduces the velocity and temperature gradient, whereas increasing the curvature factor increases the thermal gradient and velocity within the boundary. Poply (2021) evaluated the influence of MHD flux over an extending cylinder with a heat source. Their research aided in controlling the frequency of energy transmission and flow stream in a variety of industrial applications and manufacturing processes to achieve the desired end production efficiency. The influence of MHD Newtonian nanofluid flow across a stretchable cylinder was inspected by Waqas et al. (2021). The fallouts reveal that the velocity is increased by increasing the buoyancy constraint and declines by increasing the magnetic parameter. Chu et al. (2022b) analyzed the Maxwell MHD NF flow over a prolonged cylinder using nonlinear heat emission. An incompressible and 2D flow of viscoelastic NF over an extended cylinder was considered by Al-Mubaddel et al. (2022). Dey et al. (2021) investigated boundary layer viscous fluid flow via a stretchable cylinder with varying heat flux and molecular diffusion. They observed that due to the stretching of the cylinder, dual solutions are discovered, and an unusual increase in heat near the cylinder's surface. Energy consumption has grown exponentially over the world, demanding more efficient energy use because the demand exceeds the supply. Within a thermal system, a significant quantity of temperature is generated, needing efficient and rapid heat transfer employing high-performance thermal management systems. Some new efforts have been documented by many academics on fluid flow across different configurations (Chu et al., 2021; Zhao et al., 2021; Benhacine et al., 2022; Kumar and Sahu, 2022; Lim et al., 2022).

Many modern technological applications that previously required ordinary fluids (water, engine oil, ethylene glycol, and propylene glycol) have been replaced with nanofluids, which are the composition of the base fluid with nano-sized particles (Alsallami et al., 2022; Bhatti et al., 2022a; Rafiei et al., 2022). Nanofluids have garnered a huge interest in research and development in the last decade, especially in the fields of heat assignment improvement techniques and renewable and sustainable energy systems. Solar collectors, hydrodynamics, hydropower rotors, thermodynamics, ocean power plants, wind turbines, and geothermal heat exchangers are just a few of the applications for nanofluids (Ma et al., 2021). A new mechanism of thermal expansion within nanofluids has recently been introduced. The process involves mixing two or more different nanoparticles in the primary fluid. These nanofluids are referred to as hybrid nanofluids, and they have a higher heat transfer efficiency due to their improved thermo-physical properties. Propagation of the HNF flow and heat and mass transport play essential roles in biotechnology, crude oils, nuclear sectors, paper manufacturing, suspended and colloidal solutions, polyethylene solution, geophysics, unusual lubricants, and chemical plants, which are only some of the uses in the industry (Kumar et al., 2022). The fluid flow of a blood-based HNF with variable viscosity and CNTs via a stretching sheet was discovered by Chu et al. (2022a). The inclusion of CNTs proved to be more successful, according to their findings. Shruthy and Mahanthesh (2019) discussed the thermal Bénard convection analytically in HNF and Casson fluid. It has been discovered in their finding that using a hybrid nanofluid to postpone convection can improve the rate of heat allocation. A two-dimensional time-dependent radiative Casson fluid flow across a porous stretched superficial is examined by Zhou et al. (2021). They discovered that as the Casson component and magnetic field rise, the friction drags increase, whereas the Nusselt number drops with increasing Eckert number. Syam Sundar et al. (2015) measured the heat exchange ratio and friction coefficient for CNT- Fe_3O_4/water HNF flow through a cylinder under constant heat flux. Soran et al. Lung et al. (2021) evaluated the efficacy of carboxylic-synthesized CNTs modified with Fe and Mn metal to remove two pesticides from an aqueous medium. Their findings demonstrate that the CNT-COOH/MnO_2/Fe_3O_4 NPs are a viable adsorbent for the removal of pesticides from wastewater. The NPs' shape characterization and the heat transfer characteristics of an

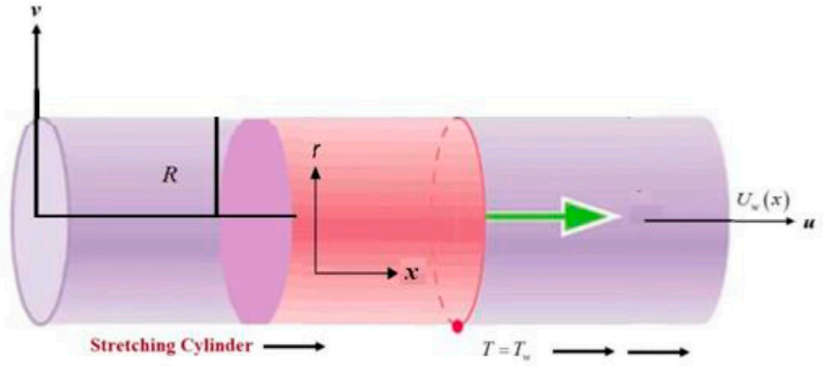

FIGURE 1
Fluid flow over a stretching cylinder.

Au–Fe_3O_4–blood HNF flowing across a stretching surface over a magnetohydrodynamic medium were presented by Ullah et al. (2019). The thermal conductivity of blade-shaped Au and Fe_3O_4 nanoparticles is found to be superior to platelet, needle, cylinder, brick, and sphere shapes. To create blood-based HNF, Mohamed et al. (2021) quantitatively studied $CoFe_2O_4$ and Fe_3O_4 ferroparticles embedded in Casson fluid, which resembles human blood. According to their findings, when magnetic effects were present, the CNT-based Casson NF flow offered 46% more heat than blood-based NF. Many scholars have recently studied hybrid nanofluid flow comprised of CNTs and iron oxide nanoparticles (Alharbi et al., 2022; Bhatti et al., 2022b; Elattar et al., 2022; Khashi'ie et al., 2022; Nazeer et al., 2022; Ullah et al., 2022).

Bioconvection has a huge involvement in manufacturing and medicine (Areekara et al., 2021; Khan et al., 2021). Elayarani et al. (2021) described the adaptive neuro-fuzzy inferential simulations for the unsteady 2D bio-convective flow of Carreau NF containing gyrotactic microbes over an elongating sheet with magnetism and multiple slip conditions. Hosseinzadeh et al. (2020) explored cross-fluid flow on a horizontal and 3D cylinder with gyrotactic microbes and NPs while accounting for viscous dissipation and magnetic field. Muhammad et al. (2021) evaluated the flow of magnetized viscoelastic Carreau NF carrying microbes through a sliding wedge with slip effects and thermal radiation parameters. Waqas et al. Muhammad et al. (2022) considered the features of the Jeffrey nanofluid flow over a sheet and the effects of activation energy and motile microorganisms. It was observed that the bioconvection Rayleigh number and resistance ratio parameter play an essential role in the Jeffery nanofluid's falling flow. Ahmad et al. (2022) investigated the novel properties of hybrid nanofluids such as $NiZnFe_2O_4$ and $MnZnFe_2O_4$. Recently, gyrotactic microorganism fluid flow and the comprising nanoparticles have been reported by Alhowaity et al. (2022b), Ashraf et al. (2022), and Habib et al. (2022).

The current research focuses on the amazing evaluation of CNTs and iron oxide-based HNF flow with magnetic dipole and triple stratification over an extending cylinder. Viscous dissipation, heat radiation, generalized Fick's law, and partial slide are also taken into account. The proposed study is significant because it examines the chemically reactive CNTs + Fe_3O_4/water Casson hybrid nanofluid with magnetic dipole and stratification effects created by an elongating cylinder. To the best of our experience, no previous research has looked into these impacts. The MATLAB function PCM and bvp4c have been used to estimate the numerical simulation of the current analysis. Graphs depict the effects of various parameters, while tables show the statistical valuation of skin friction, Nusselt number, and microorganisms .

Mathematical formulation

Over an extending cylinder, we addressed a 2D laminar and radiative Casson HNF flow in the presence of slip and microbe effects. The CNTs and iron oxide are described as NPs in the Casson fluid. The magnetic effect B_0 is executed in the r-direction. The temperature, concentration, and microorganism are symbolized as T_w, C_w, and N_w, respectively. Under the aforementioned description, the leading equations are expressed as (Ahmad et al., 2021)

$$\frac{\partial(ru)}{\partial x} + \frac{\partial(rv)}{\partial r} = 0, \tag{1}$$

$$v\frac{\partial u}{\partial x} + v\frac{\partial u}{\partial r} = \frac{\mu_{hnf}}{\rho_{hnf}}\left(1 + \frac{1}{\beta}\right)\left(\frac{\partial^2 u}{\partial r^2} + \frac{1}{r}\frac{\partial u}{\partial r}\right) + \frac{\mu_0}{\rho_{hnf}}M\frac{\partial H}{\partial x} - \nu_{hnf}\frac{u}{k^*} - \frac{C_b}{\sqrt{k^*}}u^2, \tag{2}$$

$$u\frac{\partial T}{\partial x}+v\frac{\partial T}{\partial r}=\alpha_{hnf}\left(\frac{\partial^2 T}{\partial r^2}+\frac{1}{r}\frac{\partial T}{\partial r}\right)-\mu_0 T\frac{\partial M}{\partial T}\left(u\frac{\partial H}{\partial x}+\frac{v}{r}\frac{\partial H}{\partial r}\right)+\frac{1}{\left(\rho C_p\right)_{hnf}}\left\{\mu_{hnf}\left(1+\frac{1}{\beta}\right)\left(\frac{\partial u}{\partial y}\right)^2+\frac{16\sigma^* T_\infty^3}{3k^*}\left(\frac{\partial^2 T}{\partial r^2}+\frac{1}{r}\frac{\partial T}{\partial r}\right)\right\}, \quad (3)$$

$$u\frac{\partial C}{\partial x}+v\frac{\partial C}{\partial r}=\left(D_B\right)_{hnf}\left(\frac{\partial^2 C}{\partial r^2}+\frac{1}{r}\frac{\partial C}{\partial r}\right)-k\left(C-C_\infty\right)-\lambda_c\left(v\frac{\partial v}{\partial r}\frac{\partial C}{\partial r}+v\frac{\partial u}{\partial r}\frac{\partial C}{\partial x}+u\frac{\partial v}{\partial r}\frac{\partial C}{\partial r}+u\frac{\partial u}{\partial r}\frac{\partial C}{\partial x}+2uv\frac{\partial^2 C}{\partial x\partial r}+u^2\frac{\partial^2 C}{\partial x^2}+v^2\frac{\partial^2 C}{\partial r^2}\right), \quad (4)$$

$$u\frac{\partial N}{\partial x}+v\frac{\partial N}{\partial r}+\frac{bW_c}{C_w-C_0}\frac{\partial}{\partial r}\left(N\frac{\partial C}{\partial r}\right)=\left(D_m\right)_{hnf}\left(\frac{\partial^2 N}{\partial r^2}+\frac{1}{r}\frac{\partial N}{\partial r}\right). \quad (5)$$

Here, (u, v) determine the velocity factors in the x and r direction, respectively, while μ_{hnf} is the dynamic viscosity, α_{hnf} is the thermal diffusivity, $(D_B)_{hnf}$ is the mass diffusivity, ρ_{hnf} is the density, $(D_m)_{hnf}$ is the microorganism diffusivity, λ_c is the concentration relaxation time, and w_1 is the slip factor. Additionally, $\mu_0 T\partial M/\partial T$ denotes the ferromagnetic force.

The boundary conditions are expressed as (Ahmad et al., 2021)

$$u=U_w+\nu_{hnf}w_1\left(1+\frac{1}{\beta}\right)\frac{\partial u}{\partial r}, v=0, C=C_0+\frac{bx}{l},$$

$$T=T_0+\frac{bx}{l}, N_0+\frac{bx}{l}=N \text{ at } r=R, u\to 0, C\to C_\infty$$
$$=C_0+\frac{ex}{l}, T\to T_\infty=T_0+\frac{cx}{l}, N_0+\frac{a_1 x}{l}$$
$$=N\to N_\infty \text{ when } r\to\infty\,. \quad (6)$$

In the aforementioned equation, l specifies the magnetic strength. ν_{hnf} shows the kinematic viscosity of the hybrid nanofluid, while a, b, c, d, and a_1 are the constant number.

The magnetic dipole is specified as

$$\Omega=\frac{xl}{2\pi\left(x^2+(r+c)^2\right)}, \quad (7)$$

$$\frac{\partial H}{\partial x}=-\frac{\partial\Omega}{\partial x}=\frac{x^2-(r+c)^2}{2\pi\left(x^2+(r+c)^2\right)^2}, \quad (8a)$$

$$\frac{\partial H}{\partial r}=-\frac{\partial\Omega}{\partial x}=\frac{2x(r+c)}{2\pi\left(x^2+(r+c)^2\right)^2}. \quad (8b)$$

The absolute magnetic field is

$$H=\sqrt{\left(\frac{\partial H}{\partial x}\right)^2+\left(\frac{\partial H}{\partial r}\right)^2}, \quad (9a)$$

where,

$$\frac{\partial H}{\partial x}=\frac{2x}{2\pi(r+c)^4}, \quad (9b)$$

and

$$\frac{\partial H}{\partial r}=\frac{1}{2\pi}\left(\frac{-2}{(r+c)^3}+\frac{4x}{(r+c)^5}\right). \quad (10)$$

The magnetic field became more intense, and a linear link between magnetic and temperature variation was formed as follows :

$$M=K^*\left(T-T_\infty\right). \quad (11)$$

Similarity transformation

The similarity variables are (Ahmad et al., 2021)

$$u=U_w f'(\eta), v=-\frac{R}{r}\sqrt{\frac{\nu_f U_0}{l}}f(\eta), \theta(\eta)=\frac{T-T_\infty}{T_w-T_0},$$

$$g(\eta)=\frac{C-C_\infty}{C_w-C_0}, h(\eta)=\frac{N-N_\infty}{N_w-N_0}, \quad \eta=\frac{r^2-R^2}{2R}\sqrt{\frac{U_w}{\nu_f l}}. \quad (12)$$

By applying the aforementioned similarity transformation, Eq. 1 is identically satisfied while Eqs 2–5 take the form as

$$\left(\frac{\left(1+\frac{1}{\beta}\right)}{A_1A_2}\right)\left((1+2\alpha\eta)f'''+2\alpha f''\right)+ff''-Fr\left(f'\right)^2-\frac{2M\theta}{\left(\eta+\gamma_1\right)^4A_2}=0, \quad (13)$$

$$\left(\frac{k_{hnf}}{k_f}+\frac{4}{3}Rd\right)\left((1+2\alpha\eta)\theta''+2\theta'\alpha\right)+Pr\left(f\theta'-S_1f'-2f'\theta+Ec\left(1+\frac{1}{\beta}\right)f''^2\right)-\frac{2\lambda M(\theta-\epsilon)f}{\left(\gamma_1+\eta\right)^3}-2\lambda f'^2=0, \quad (14)$$

$$\frac{A_1}{S_c}\left((1+2\alpha\eta)g''+2\alpha g'\right)+fg'-2Crgf'-S_2f'-\gamma_c\left(f^2g''+ff'g'\right)=0, \quad (15)$$

$$A_1\left((1+2\alpha\eta)hh''+2\alpha h'\right)+L_b\left(fh'-S_3f'-2f'h\right)-P_e\left(g'h'+(h+\delta)\left((1+2\alpha\eta)g''+2\alpha g'\right)\right)=0. \quad (16)$$

The reduced boundary conditions are

$$f(0)=0, f'(0)=1+\left(1+\frac{1}{\beta}\right)\frac{s}{A_1}f''(0), \theta(0)=1-S_1,$$

$$g(0)=1-S_2, h(0)=1-S_3, f'(\infty)\to 0, \theta(\infty)\to 0, h(\infty)\to 0, g(\infty)\to 0. \quad (17)$$

Here, S_3 is the microorganism stratification, α is the curvature term, δ the bio-convection constant, β is the Casson fluid constraints, S_1 is the thermal stratification, M is the ferromagnetic term, S_2 is the concentration stratification, Ec is the Eckert number, s is the velocity slip, Rd is the radiation constant, Pe is the Peclet number, ϵ is the free stream parameter, Lb is the Lewis number, Pr is the Prandtl number, Sc is the Schmidt number, γ_c is the concentration relaxation constraints, Cr is the chemical reaction term, and λ is the viscous dissipation parameter.

These physical terms are expressed as (Ahmad et al., 2021)

$$s=w_1\left(\frac{U_0\nu_f}{l}\right), Lb=\frac{\nu_f}{D_m}, Pr=\frac{\nu_f}{\alpha_f}, S_1=\frac{c}{b}, Pe=\frac{bW_c}{D_m},$$

$$S_2 = \frac{e}{d}, S_c = \frac{\upsilon_f}{D_b}, \alpha = \sqrt{\frac{l\nu_f}{U_0}}, S_3 = \frac{a_1}{a}, M = \frac{\rho_f \gamma_1 \mu_0 K^* (T_0 - T_w)}{2\pi\mu_f}, Ec = \frac{U_0^2}{c_p (T_w - T_\infty)}, \gamma_1 = \sqrt{\frac{\rho_f U_0 b^2}{\mu_f}}, \delta = \frac{N_\infty}{N_w - N_\infty}, \lambda = \frac{\mu_f^2 U_2}{\rho_f k (T_0 - T_w)}. \Bigg\} \quad (18)$$

The physical interest quantities derived from the present study are

$$Nn_x = \frac{xq_n}{D_m (n_w - n_\infty)}, Sh_x = \frac{xq_m}{D_B (C_w - C_\infty)}, Nu_x = \frac{xq_w}{k_f (T_w - T_\infty)}, C_f = \frac{2\tau_w}{\rho_f u_w^2}. \quad (19)$$

The non-dimensional forms of the physical quantities are

$$Nn_x \mathrm{Re}_x^{\frac{-1}{2}} = -h'(0), Sh_x \mathrm{Re}_x^{\frac{-1}{2}} = -g'(0), Nu_x \mathrm{Re}_x^{\frac{-1}{2}} = -\frac{k_{hnf}}{k_f}\theta'(0), C_f \mathrm{Re}_x^{\frac{1}{2}} = -\frac{1}{A_1}\left(1 + \frac{1}{\beta}\right) f''(0). \quad (20)$$

Numerical solution

Many researchers have used different numerical, computational, and numerical procedures to solve nonlinear systems of PDEs (Jin et al., 2022; Rashid et al., 2022a; Rashid et al., 2022b; Wang et al., 2022; Zhao et al., 2022). Here, the problem is handled through the PCM methodology, which is operated as follows (Berezowski, 2010; Shuaib et al., 2020; Jin et al., 2022; Rashid et al., 2022a; Rashid et al., 2022b; Sun et al., 2022; Wang et al., 2022; Zhao et al., 2022):

Step 1: Reducing Eqs 13–16 to first order

$$\left.\begin{aligned}\zeta_1 = f(\eta), \zeta_2 = f'(\eta), \zeta_3 = f''(\eta), \zeta_4 = \theta(\eta), \zeta_5 = \theta'(\eta), \zeta_6 \\ = g(\eta), \zeta_7 = g'(\eta), \zeta_8 = h(\eta) \zeta_9 = h'(\eta).\end{aligned}\right\} \quad (21)$$

By putting Eqs 21 in Eqs 13–17, we get

$$\left(\frac{\left(1+\frac{1}{\beta}\right)}{A_1 A_2}\right)(1 + 2\alpha\eta)\zeta_3' + \left(2\alpha\left(\frac{\left(1+\frac{1}{\beta}\right)}{A_1 A_2}\right) + \zeta_1\right)\zeta_3 - Fr(\zeta_2)^2 - \frac{2M\zeta_4}{(\eta + \gamma_1)^4 A_2} = 0, \quad (22)$$

$$\left(\frac{k_{hnf}}{k_f} + \frac{4}{3}Rd\right)(1 + 2\alpha\eta)\zeta_5' + \left(2\alpha\left(\frac{k_{hnf}}{k_f} + \frac{4}{3}Rd\right) + Pr\zeta_1\right)\zeta_5 + Pr\begin{pmatrix}-2\zeta_2\zeta_4 - S_1\zeta_2 \\ +Ec\left(1 + \frac{1}{\beta}\right)\zeta_3^2\end{pmatrix} - \frac{2\lambda M(\zeta_4 - \epsilon)\zeta_1}{(\gamma_1 + \eta)^3} - 2\lambda\zeta_2^2 = 0, \quad (23)$$

$$\left(\frac{A_1}{S_c}(1 + 2\alpha\eta) - \gamma_c\zeta_1^2\right)\zeta_7' + \left(\frac{A_1}{S_c}2\alpha + f - \gamma_c\zeta_1\zeta_2\right)\zeta_7 - 2Cr\zeta_6\zeta_2 - S_2\zeta_2 = 0, \quad (24)$$

$$A_1(1 + 2\alpha\eta)\zeta_9' + (A_1 2\alpha + L_b\zeta_1 - P_e\zeta_7)\zeta_9 - L_b(2\zeta_2\zeta_8 - S_3\zeta_2) - P_e\left((\zeta_8 + \delta)\begin{pmatrix}(1 + 2\alpha\eta) \\ \zeta_7' + 2\alpha\zeta_7\end{pmatrix}\right) = 0, \quad (25)$$

with the corresponding boundary conditions.

$$\zeta_1(0) = 0, \zeta_2(0) = 1 + \left(1 + \frac{1}{\beta}\right)\frac{s}{A_1}\zeta_3(0), \zeta_4(0) = 1 - S_1,$$

$$\zeta_6(0) = 1 - S_2, \zeta_8(0) = 1 - S_3, \zeta_2(\infty) \to 0, \zeta_4(\infty) \to 0, \zeta_6(\infty) \to 0, \zeta_8(\infty) \to 0. \quad (26)$$

Step 2: Familiarizing parameter p in Eqs 22–26:

$$\left(\frac{\left(1+\frac{1}{\beta}\right)}{A_1 A_2}\right)(1 + 2\alpha\eta)\zeta_3' + \left(2\alpha\left(\frac{\left(1+\frac{1}{\beta}\right)}{A_1 A_2}\right) + \zeta_1\right)((\zeta_3 - 1)p + 1) - Fr(\zeta_2)^2 - \frac{2M\zeta_4}{(\eta + \gamma_1)^4 A_2} = 0, \quad (27)$$

$$\left(\frac{k_{hnf}}{k_f} + \frac{4}{3}Rd\right)(1 + 2\alpha\eta)\zeta_5' + \left(2\alpha\left(\frac{k_{hnf}}{k_f} + \frac{4}{3}Rd\right) + Pr\zeta_1\right)((\zeta_5 - 1)p + 1) + Pr\begin{pmatrix}-2\zeta_2\zeta_4 - S_1\zeta_2 \\ +Ec\left(1 + \frac{1}{\beta}\right)\zeta_3^2\end{pmatrix} - \frac{2\lambda M(\zeta_4 - \epsilon)\zeta_1}{(\gamma_1 + \eta)^3} - 2\lambda\zeta_2^2 = 0, \quad (28)$$

$$\left(\frac{A_1}{S_c}(1 + 2\alpha\eta) - \gamma_c\zeta_1^2\right)\zeta_7' + \left(\frac{A_1}{S_c}2\alpha + f - \gamma_c\zeta_1\zeta_2\right)((\zeta_7 - 1)p + 1) - 2Cr\zeta_6\zeta_2 - S_2\zeta_2 = 0, \quad (29)$$

$$A_1(1 + 2\alpha\eta)\zeta_9' + (A_1 2\alpha + L_b\zeta_1 - P_e\zeta_7)((\zeta_9 - 1)p + 1) - L_b(2\zeta_2\zeta_8 - S_3\zeta_2) - P_e\left((\zeta_8 + \delta)\left((1 + 2\alpha\eta)\zeta_7' + 2\alpha\zeta_7\right)\right) = 0. \quad (30)$$

Step 3: Applying the Cauchy Principal and discretizing Eqs 27–30.

After discretization, the obtained set of equations is computed through Matlab code of PCM.

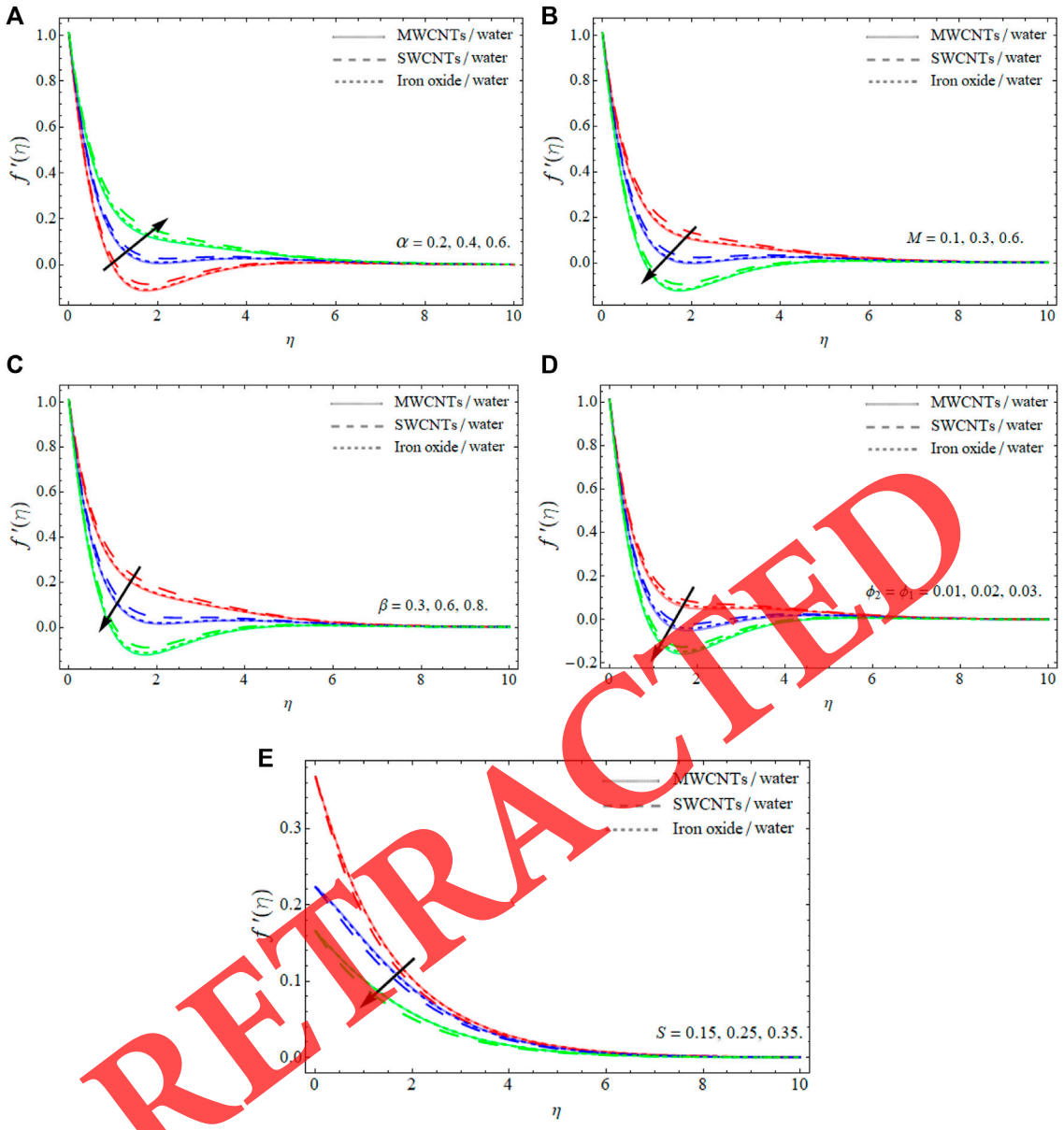

FIGURE 2
Effects of curvature parameter α, ferromagnetic parameter M, fluid parameter β, volume fraction ϕ_1, and slip parameter S on velocity profile $f'(\eta)$.

Results and discussion

For hybrid NF consisting of CNTS and magnetic ferrite NPs, the discussion section examines the comportment of velocity, energy, and motile microbe profile against the change of numerous physical restrictions. The comparative Figures 2–5 and Tables 2–4 exhibit their outcomes.

Figure 1 illustrates the physical mechanism of fluid flow over a stretching cylinder. Figures 2A–E exemplify the variations in the velocity profile for the curvature parameter α, ferromagnetic parameter M, fluid parameter β, volume fraction ϕ_1, and slip parameter S, respectively. The results indicate that the velocity field shows a reducing trend for the enhanced values of the curvature constraint. It is observed in the result that as the curvature factor is increased, the radius of the cylinder shrinks which produces minimal resistance to fluid flow, and therefore, the fluid velocity increases. The decreasing behavior of the velocity profile for the variation of ferromagnetic parameter M can be seen in Figure 2B. The reason for this decline is that when the ferromagnetic

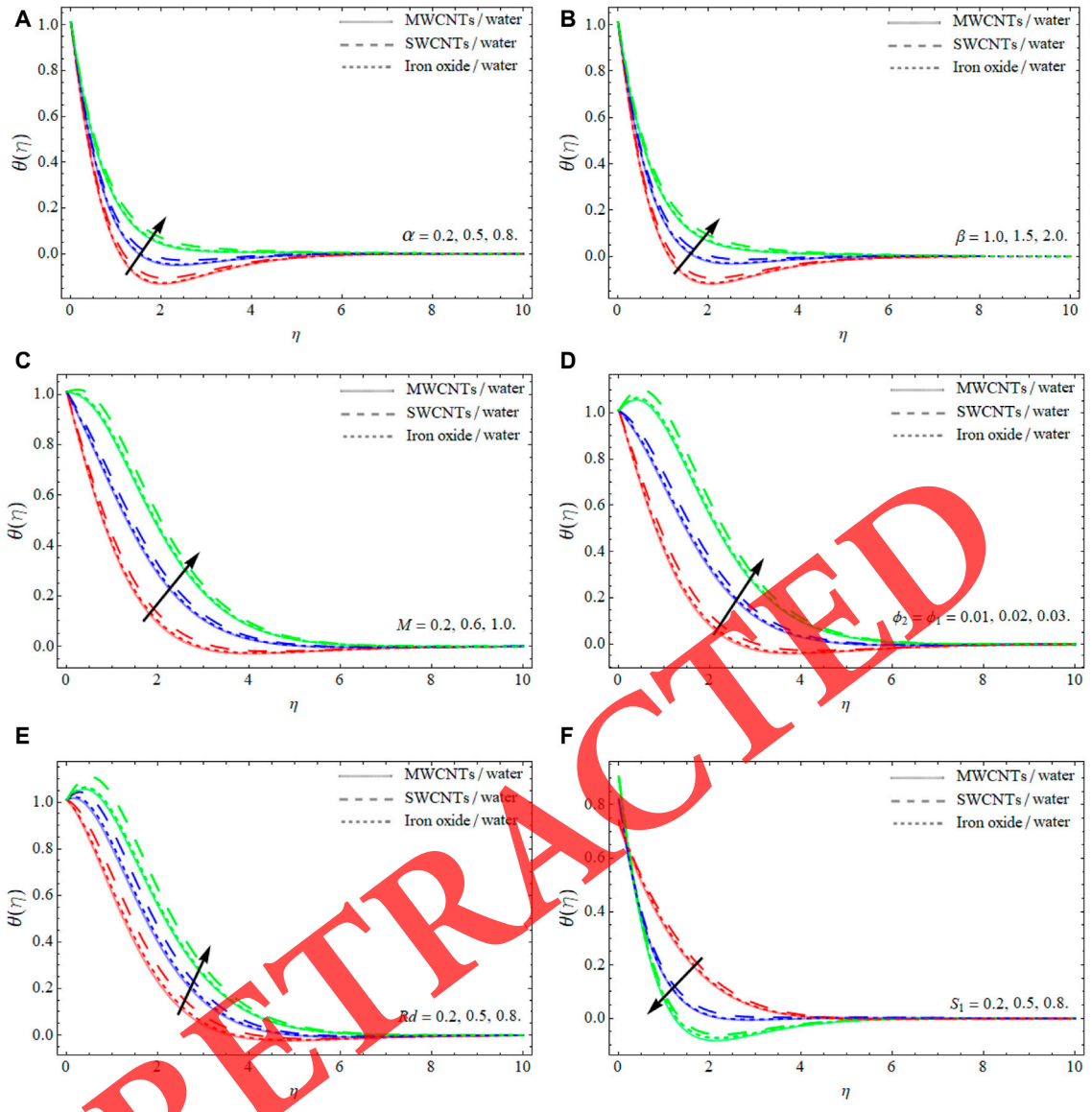

FIGURE 3
Effects of curvature parameter α, fluid parameter β, ferromagnetic M, volume fraction ϕ_1 , thermal radiation Rd, and thermal stratification S_1 on energy profile $\theta(\eta)$.

parameter increases, a stronger resistive force arises known as Lorentz force which decreases the fluid velocity. The velocity profile displays a declining behavior for the rising values of the Casson fluid factor, as shown in Figure 2C. The reason behind this decline is that as the Casson parameter increases, the fluid acts like a Newtonian fluid which reduces the velocity field. Figure 2D shows the upshot of ϕ_1 on $f'(\eta)$. Higher valuation of ϕ_1 diminishes the velocity $f'(\eta)$ field. By expanding the volume percentage, the transit, adhesive force, and excitation energy across CNTs and Fe_3O_4 NF reduce, resulting in a drop in the velocity field. Figure 2E shows the upshot of the velocity slip constraint S on the fluid velocity. The graph indicates the decrease in the fluid velocity due to growing values of S. It is due to velocity difference between near the surface and away from the cylinder.

The influence of α, β, M, ϕ_1, Rd, and S_1 on the energy profile is shown in Figures 3A–F. The impact of the curvature on the energy outlines $\theta(\eta)$ is seen in Figure 3A. The heat transfer improves as the values of α improve, as seen in the figures. Physically, as the curvature term upsurges, the radius of the cylinder expands, due to which the maximum number of NPs are attached to the surface of the cylinder, which transmits more heat, so the temperature field improves. Figure 3B shows influence of β (Casson fluid) on the energy contour $\theta(\eta)$. The

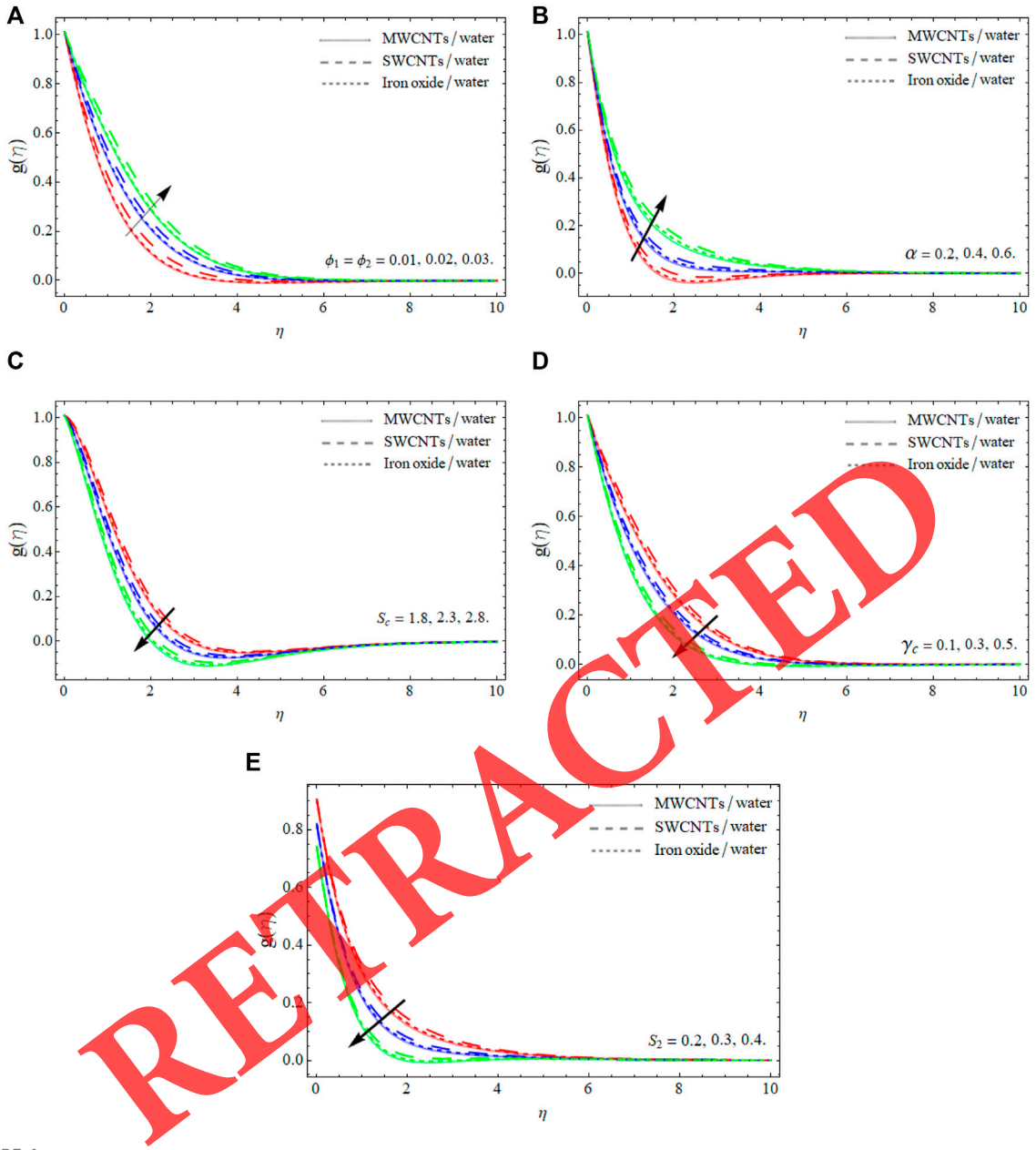

FIGURE 4
Effects of volume fraction ϕ_1, curvature parameter α, Schmidt number S_c, the concentration relaxation parameter γ_c, and concentration stratification parameter S_2 on concentration profile $g(\eta)$.

temperature distribution improves with improved β values, as shown in the figure. It is shown that the Casson term is in an inverse relation to the yield stress. The influence of the magnetic coefficient M and ϕ_1 on the energy dispersal is seen in Figures 3C,D. Improvement in the fluid temperature corresponded to rises in the magnetic effect M and solid volume fraction parameter ϕ_1, as seen in the figures. A resistive pressure is created when the magnetic field is improved, which raises the temperature of the fluid. In Figure 3E, the effect of the radiation term Rd on the fluid's temperature field is investigated. As the radiation number upsurges, the fluid temperature rises. When the radiation term is increased, the fluid absorbs more heat, causing the fluid temperature to rise. The impact of thermal stratification parameter S_1 is shown in Figure 3F. It is to be noted that the energy profile decreases for larger values of S_1.

The effects ϕ_1, α, S_c, γ_c, and S_2 on concentration profile $g(\eta)$ are shown in Figures 4A–E. Figure 4A shows the influence of the

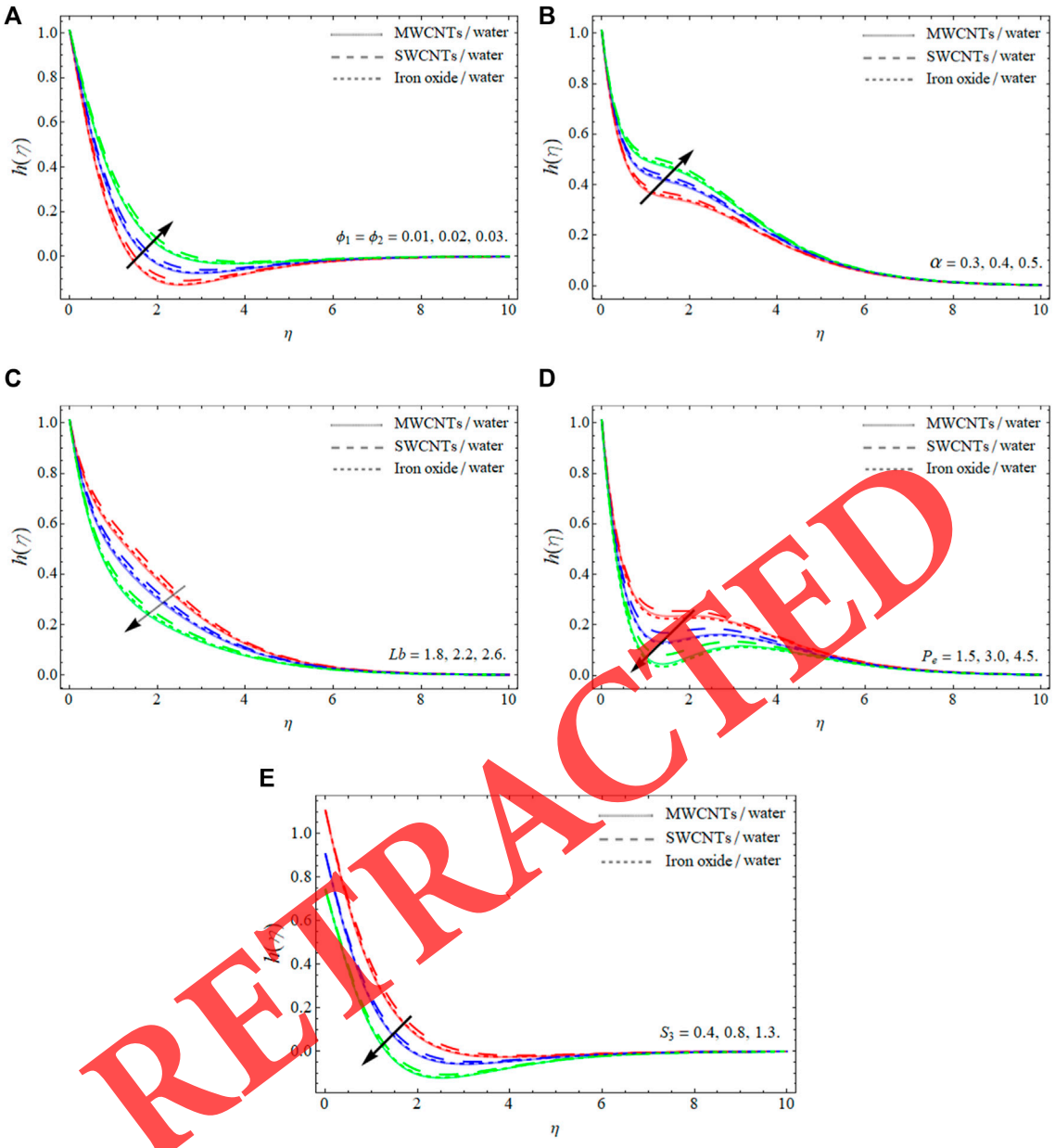

FIGURE 5
Effects of volume fraction ϕ_1, curvature parameter α, bio-convection Lewis number *Lb*, Peclet number *Pe*, and the microorganism stratification parameter S_3, on microorganism profile $h(\eta)$.

volume fraction indicator ϕ_1 for both CNTs and iron ferrite NF on the mass profile. Because the fluid average viscosity becomes dense as the quantity of iron oxide NPs and CNTs increases, the mass transfer rate slows. As a result, as credit ϕ_1 grows, the concentration profile decreases. Figure 4B shows that the curvature parameter α is a decreasing function of mass transfer $g(\eta)$. The mass transmission rate reduces with increases in α. Figure 4C indicates the influence of the concentration profile. By increasing the values of S_c, the

TABLE 1 Experimental values of water, *CNTs*, and Fe_3O_4 nanoparticles (Gul et al., 2020).

	ρ (kg/m^3)	C_p (j/kgK)	k (W/mK)
Pure water	997.1	4,179	0.613
SWCNTs	2,600	425	6,600
MWCNTs	1,600	796	300
Fe_3O_4	5, 200	670	6

TABLE 2 Thermo-physical relations of hybrid nanofluids (Gul et al., 2020).

Properties	
Viscosity	$\mu_{hnf}/\mu_{bf} = 1/(1-\phi_{Fe_3O_4}-\phi_{CNT})^2$
Density	$\frac{\rho_{hnf}}{\rho_{bf}} = \phi_{Fe_3O_4}(\rho_{Fe_3O_4}/\rho_{bf}) + \phi_{CNT}(\rho_{CNT}/\rho_{bf}) + (1-\phi_{Fe_3O_4}-\phi_{CNT})$
Thermal capacity	$(\rho C_p)_{hnf}/(\rho C_p)_{bf} = \phi_{Fe_3O_4}((\rho C_p)_{Fe_3O_4}/(\rho C_p)_{bf}) + \phi_{CNT}((\rho C_p)_{CNT}/(\rho C_p)_{bf}) + (1-\phi_{Fe_3O_4}-\phi_{CNT})$
Thermal conductivity	$\frac{k_{hnf}}{k_{bf}} = [(\phi_{Fe_3O_4}k_{Fe_3O_4} + \phi_{CNT}k_{CNT}/\phi_{Fe_3O_4} + \phi_{Fe_2O_4}) + 2k_{bf} + 2(\phi_{Fe_3O_4}k_{Fe_3O_4} + \phi_{CNT}k_{CNT}) - 2(\phi_{Fe_3O_4} + \phi_{CNT})k_{bf}/(\phi_{Fe_3O_4}k_{Fe_3O_4} + \phi_{CNT}k_{CNT}/\phi_{Fe_3O_4} + \phi_{CNT}) + 2k_{bf} - 2(k_{Fe_3O_4}\phi_{Fe_3O_4} + k_{CNT}\phi_{CNT}) + (\phi_{Fe_3O_4} + \phi_{CNT})2k_{bf}]$
Electrical conductivity	$\frac{\sigma_{hnf}}{\sigma_{bf}} = [(\phi_{Fe_3O_4}\sigma_{Fe_3O_4} + \sigma_{CNT}\phi_{CNT}/\phi_{Fe_2O_4} + \phi_{Fe_3O_4}) + 2\sigma_{bf} + 2(\phi_{Fe_3O_4}\sigma_{Fe_3O_4} + \phi_{CNT}\sigma_{CNT}) - 2(\phi_{Fe_3O_4} + \phi_{CNT})\sigma_{bf}/(\phi_{Fe_3O_4}\sigma_{Fe_3O_4} + \phi_{CNT}\sigma_{CNT}/\phi_{Fe_2O_4} + \phi_{CNT}) + 2\sigma_{bf} - (\phi_{Fe_3O_4}\sigma_{Fe_3O_4} + \phi_{CNT}\sigma_{CNT}) + (\phi_{Fe_3O_4} + \phi_{CNT})\sigma_{bf}]$

TABLE 3 Numerical outcomes of $C_f\mathrm{Re}_x^{1/2}$, $Sh_x\mathrm{Re}_x^{-1/2}$, $Nu_x\mathrm{Re}_x^{-1/2}$, and $Nn_x\mathrm{Re}_x^{-1/2}$ when $\beta \to \infty$.

M	α	ϕ_1	$C_f\mathrm{Re}_x^{1/2}$	$Sh_x\mathrm{Re}_x^{-1/2}$	$Nu_x\mathrm{Re}_x^{-1/2}$	$Nn_x\mathrm{Re}_x^{-1/2}$
0	0.1	0.01	0.948817	1.474229	1.392515	2.613915
0.2	0.1		1.019293	1.472838	1.374741	2.609771
0.5	0.1		1.114171	1.471116	1.350623	2.604243
1.0	0.1		1.251316	1.468902	1.315447	2.596366
	0.0		0.951866	1.345417	1.360632	2.589183
	0.2		1.017015	1.500974	1.406222	2.634011
	0.5		1.108962	1.579961	1.474076	2.698487
	0.7		1.251286	1.701900	1.583912	2.799354
		0.01	0.916480	1.456307	1.312150	2.604988
		0.02	0.922977	1.460090	1.328514	2.606844
		0.03	0.984888	1.473504	1.383434	2.611791
		0.04	1.134798	1.487764	1.453457	2.619460

TABLE 4 Statistical outcomes of microorganism transmission rate $-h'(0)$.

Lb	Pe	α	δ	$-h'(0)$	
				SWCNTs	MWCNTs
0.5	0.5	0.1	0.1	1.6591	1.6606
0.6				1.7422	1.7439
0.7				1.8210	1.7227
0.5	0.1			1.3693	1.3707
	0.2			1.5329	1.5345
	0.3			1.6987	1.7003
	0.5	0.2		2.0662	2.0679
		0.3		2.0962	2.0978
		0.4	0.2	2.1262	2.1278
			0.3	2.0996	2.1014
			0.4	2.1631	2.1649
			0.5	2.2267	2.2285

concentration profile decreases. Because increasing the value of Sc lowers the mass permeability, the mass rate falls. Figure 4D depicts the variance in the concentration profile sketch as a function of various estimations of the concentration relaxation. It is stated that a higher mass relaxation factor approximation lowers the concentration profile. The effect of the

concentration stratification coefficient on the concentration distribution is shown by Figure 4E. The augmentation of the concentration stratification factor results in a diminution in the sketch and the related boundary layer thickness.

Figures 5A,B show the consequences of ϕ_1 and α on the microbial density sketch. The microorganism frequency and corresponding boundary layer thickness show an increasing tendency for larger values of ϕ_1 and α, as shown in Figures 5A,B. Figures 5C–E show that the effect of Lb, P_e, and S_3 on $h(\eta)$ declines the motile microorganism profile. Physically, Lb is in an inverse relation with the mass diffusion and an increase in Lb results in the reduction of $h(\eta)$. Additionally, it is observed that rising values of P_e destabilize the gyrotactic microbes' profile and a higher P_e enhances the progress of NF flow.

Tables 1, 2 revealed the experimental values of base fluid and nanoparticles and the mathematical model used for the proposed model. Table 3 shows the statistical assessments of skin friction $C_f \mathrm{Re}_x^{1/2}$, mass transfer $Sh_x \mathrm{Re}_x^{-1/2}$, heat transfer rate $Nu_x \mathrm{Re}_x^{-1/2}$, and motile microorganism transmission rate $Nn_x \mathrm{Re}_x^{-1/2}$. Table 4 shows the comparative analysis between SWCNTs and MWCNTs for the microorganism transfer rate.

Conclusion

We have studied the energy and mass transfer across an expanding cylinder in a water-based Darcy–Forchheimer hybrid nanofluid flow. The influence of a magnetic field, viscous dissipation, heat source, thermal radiation, concentration stratification, and chemical reaction on fluid flow has been investigated. The phenomena are treated as a nonlinear system of PDEs. Using similarity substitution, the modeled equations are further solved through a computational approach PCM. The key findings are:

- The addition of carbon nanotubes (CNTs) and nanocrystals to the base fluid boosts heat and mass conduction remarkably.
- The velocity outlines $f'(\eta)$ significantly lower with the variation of the curvature factor, ferromagnetic effect, Casson fluid constraints, volume fraction, and slip parameter.
- The heat transport rate $\theta(\eta)$ increases with the rising values of curvature parameter, Casson fluid parameter, magnetic effect, and solid nanoparticles volume fraction, while declining with the effect of the thermal stratification parameter
- The mass transfer rate $g(\eta)$ declines with growing credit of nanoparticles, Schmidt number Sc, and concentration relaxation constraint, while enhances with the effect of the curvature term.
- The motile microorganism propagation rate boosts with variations in ϕ_1 and α, while reduces with the effect of Lb, Pe, and S_3.

Data availability statement

The original contributions presented in the study are included in the article/Supplementary Material; further inquiries can be directed to the corresponding author.

Author contributions

All authors listed have made a substantial, direct, and intellectual contribution to the work and approved it for publication.

Funding

The authors extend their appreciation to the Deanship of Scientific Research at King Khalid University for funding this work through Large Groups (RGP.2/94/43). The authors would like to thank the Deanship of Scientific Research at Umm Al-Qura University for supporting this work by Grant Code: 22UQU4282396DSR17.

Conflict of interest

The authors declare that the research was conducted in the absence of any commercial or financial relationships that could be construed as a potential conflict of interest.

Publisher's note

All claims expressed in this article are solely those of the authors and do not necessarily represent those of their affiliated organizations, or those of the publisher, the editors, and the reviewers. Any product that may be evaluated in this article, or claim that may be made by its manufacturer, is not guaranteed or endorsed by the publisher.

References

Ahmad, S., Akhter, S., Shahid, M. I., Ali, K., Akhtar, M., and Ashraf, M. (2022). Novel thermal aspects of hybrid nanofluid flow comprising of manganese zinc ferrite MnZnFeO, nickel zinc ferrite NiZnFeO and motile microorganisms. *Ain Shams Eng. J.* 13 (5), 101668. doi:10.1016/j.asej.2021.101668

Ahmad, S., Naveed Khan, M., Rehman, A., Felemban, B. F., Alqurashi, M. S., Alharbi, F. M., et al. (2021). Analysis of heat and mass transfer features of hybrid casson nanofluid flow with the magnetic dipole past a stretched cylinder. *Appl. Sci.* 11 (23), 11203. doi:10.3390/app112311203

Al-Mubaddel, F. S., Allehiany, F. M., Nofal, T. A., Alam, M. M., Ali, A., and Asamoah, J. K. K. (2022). Rheological model for generalized energy and mass transfer through hybrid nanofluid flow comprised of magnetized cobalt ferrite nanoparticles. *J. Nanomater.* 2022, 1–11. doi:10.1155/2022/7120982

Alharbi, K. A. M., Ahmed, A. E. S., Ould Sidi, M., Ahammad, N. A., Mohamed, A., El-Shorbagy, M. A., et al. (2022). Computational valuation of Darcy ternary-hybrid nanofluid flow across an extending cylinder with induction effects. *Micromachines* 13 (4), 588. doi:10.3390/mi13040588

Alhowaity, A., Hamam, H., Bilal, M., and Ali, A. Numerical study of Williamson hybrid nanofluid flow with thermal characteristics past over an extending surface. *Heat. Trans.* (2022b). doi:10.1002/htj.22616

Alsallami, S. A., Zahir, H., Muhammad, T., Hayat, A. U., Khan, M. R., and Ali, A. (2022). Numerical simulation of Marangoni Maxwell nanofluid flow with Arrhenius activation energy and entropy anatomization over a rotating disk. *Waves Random Complex Media*, 1–19. doi:10.1080/17455030.2022.2045385

Areekara, S., Mabood, F., Sabu, A. S., Mathew, A., and Badruddin, I. A. (2021). Dynamics of water conveying single-wall carbon nanotubes and magnetite nanoparticles subject to induced magnetic field: A bioconvective model for theranostic applications. *Int. Commun. Heat Mass Transf.* 126, 105484. doi:10.1016/j.icheatmasstransfer.2021.105484

Ashraf, M. Z., Rehman, S. U., Farid, S., Hussein, A. K., Ali, B., Shah, N. A., et al. (2022). Insight into significance of bioconvection on mhd tangent hyperbolic nanofluid flow of irregular thickness across a slender elastic surface. *Mathematics* 10 (15), 2592. doi:10.3390/math10152592

Benhacine, H., Mahfoud, B., and Salmi, M. (2022). Stability of conducting fluid flow between coaxial cylinders under thermal gradient and axial magnetic field. *Int. J. Thermofluid Sci. Technol.* 9 (2), 090202. doi:10.36963/ijtst.2022090202

Berezowski, M. (2010). The application of the parametric continuation method for determining steady state diagrams in chemical engineering. *Chem. Eng. Sci.* 65 (19), 5411–5414. doi:10.1016/j.ces.2010.07.003

Bhatti, M. M., Arain, M. B., Zeeshan, A., Ellahi, R., and Doranehgard, M. H. (2022a). Swimming of Gyrotactic Microorganism in MHD Williamson nanofluid flow between rotating circular plates embedded in porous medium: Application of thermal energy storage. *J Energy Storage* 45 (4), 103511. doi:10.1016/j.est.2021.103511

Bhatti, M. M., Ellahi, R., and Doranehgard, M. H. (2022b). Numerical study on the hybrid nanofluid (Co_3O_4-Go/H_2O) flow over a circular elastic surface with non-Darcy medium: Application in solar energy. *J. Mol. Liq.* 361, 119655. doi:10.1016/j.molliq.2022.119655

Chu, Y. M., Bashir, S., Ramzan, M., and Malik, M. Y. (2022a). Model-based comparative study of magnetohydrodynamics unsteady hybrid nanofluid flow between two infinite parallel plates with particle shape effects. *Math. Methods Appl. Sci.* doi:10.1002/mma.8234

Chu, Y. M., Nazir, U., Sohail, M., Selim, M. M., and Lee, J. R. (2021). Enhancement in thermal energy and solute particles using hybrid nanoparticles by engaging activation energy and chemical reaction over a parabolic surface via finite element approach. *Fractal Fract.* 5 (3), 119. Article 119. doi:10.3390/fractalfract5030119

Chu, Y. M., Shankaralingappa, B. M., Gireesha, B. J., Alzahrani, F., Khan, M. I., and Khan, S. U. (2022b). Combined impact of Cattaneo-Christov double diffusion and radiative heat flux on bio-convective flow of Maxwell liquid configured by a stretched nano-material surface. *Appl. Math. Comput.* 419, 126883. doi:10.1016/j.amc.2021.126883

Dey, D., Borah, R., and Mahanta, B. (2021). "Boundary layer flow and its dual solutions over a stretching cylinder: Stability analysis," in *Emerging technologies in data mining and information security* (Singapore: Springer), 27–38.

Dou, H. S. (2022). "Stability of taylor-couette flow between concentric rotating cylinders," *Origin of turbulence* (Singapore: Springer), 271–304.

Elattar, S., Helmi, M. M., Elkotb, M. A., El-Shorbagy, M. A., Abdelrahman, A., Bilal, M., et al. (2022). Computational assessment of hybrid nanofluid flow with the influence of hall current and chemical reaction over a slender stretching surface. *Alexandria Eng. J.* 61 (12), 10319–10331. doi:10.1016/j.aej.2022.03.054

Elayarani, M., Shanmugapriya, M., and Kumar, P. S. (2021). Intensification of heat and mass transfer process in MHD carreau nanofluid flow containing gyrotactic microorganisms. *Chem. Eng. Process. - Process Intensif.* 160, 108299. doi:10.1016/j.cep.2021.108299

Gul, T., Rahman, J. U., Bilal, M., Saeed, A., Alghamdi, W., Mukhtar, S., et al. (2020). Viscous dissipated hybrid nanoliquid flow with Darcy–Forchheimer and forced convection over a moving thin needle. *AIP Adv.* 10 (10), 105308. doi:10.1063/5.0022210

Habib, D., Salamat, N., Abdal, S., Siddique, I., Salimi, M., and Ahmadian, A. (2022). On time dependent MHD nanofluid dynamics due to enlarging sheet with bioconvection and two thermal boundary conditions. *Microfluid Nanofluid* 26, 11. doi:10.1007/s10404-021-02514-y

Hosseinzadeh, K., Roghani, S., Mogharrebi, A. R., Asadi, A., Waqas, M., and Ganji, D. D. (2020). Investigation of cross-fluid flow containing motile gyrotactic microorganisms and nanoparticles over a three-dimensional cylinder. *Alexandria Eng. J.* 59 (5), 3297–3307. doi:10.1016/j.aej.2020.04.037

Hussain, Z., Hussain, A., Anwar, M. S., and Farooq, M. (2022). Analysis of Cattaneo–Christov heat flux in Jeffery fluid flow with heat source over a stretching cylinder. *Therm. Anal. Calorim.* 147, 3391–3402. doi:10.1007/s10973-021-10573-0

Jin, F., Qian, Z. S., Chu, Y. M., and ur Rahman, M. (2022). On nonlinear evolution model for drinking behavior under Caputo-Fabrizio derivative. *jaac.* 12 (2), 790–806. doi:10.11948/20210357

Khan, S. U., Al-Khaled, K., and Bhatti, M. M. (2021). Bioconvection analysis for flow of Oldroyd-B nanofluid configured by a convectively heated surface with partial slip effects. *Surf. Interfaces* 23, 100982. doi:10.1016/j.surfin.2021.100982

Khashi'ie, N. S., Arifin, N. M., and Pop, I. (2022). Magnetohydrodynamics (MHD) boundary layer flow of hybrid nanofluid over a moving plate with Joule heating. *Alex. Eng. J.* 61 (3), 1938–1945. doi:10.1016/j.aej.2021.07.032

Kumar, D., and Sahu, A. K. (2022). Non-Newtonian fluid flow over a rotating elliptic cylinder in laminar flow regime. *Eur. J. Mech. B Fluids* 93, 117–136. doi:10.1016/j.euromechflu.2022.01.005

Kumar, L. H., Kazi, S. N., Masjuki, H. H., and Zubir, M. N. M (2022). A review of recent advances in green nanofluids and their application in thermal systems. *Chem. Eng. J.* 429, 132321. doi:10.1016/j.cej.2021.132321

Lim, Y. J., Shafie, S., Isa, S. M., Rawi, N. A., and Mohamad, A. Q. (2022). Impact of chemical reaction, thermal radiation, and porosity on free convection Carreau fluid flow towards a stretching cylinder. *Alexandria Eng. J.* 61 (6), 4701–4717. doi:10.1016/j.aej.2021.10.023

Lung, I., Soran, M. L., Stegarescu, A., and Opriş, O. (2021). Devrinol and triadimefon removal from aqueous solutions using CNT-COOH/MnO2/Fe3O4 nanocomposite. *J. Iran. Chem. Soc.* 19, 2031–2039. doi:10.1007/s13738-021-02442-2

Ma, T., Guo, Z., Lin, M., and Wang, Q. (2021). Recent trends on nanofluid heat transfer machine learning research applied to renewable energy. *Renew. Sustain. Energy Rev.* 138, 110494. doi:10.1016/j.rser.2020.110494

Ma, Y., Luan, Y., and Xu, W. (2020). Hydrodynamic features of three equally spaced, long flexible cylinders undergoing flow-induced vibration. *Eur. J. Mech. - B/Fluids* 79, 386–400. doi:10.1016/j.euromechflu.2019.09.021

Mohamed, M. K. A., Yasin, S. H. M., Salleh, M. Z., and Alkasasbeh, H. T. (2021). MHD stagnation point flow and heat transfer over a stretching sheet in a blood-based casson ferrofluid with Newtonian heating. *J. Adv. Res. Fluid Mech. Therm. Sci.* 82 (1), 1–11. doi:10.37934/arfmts.82.1.111

Muhammad, T., Alamri, S. Z., Waqas, H., Habib, D., and Ellahi, R. (2021). Bioconvection flow of magnetized Carreau nanofluid under the influence of slip over a wedge with motile microorganisms. *J. Therm. Anal. Calorim.* 143 (2), 945–957. doi:10.1007/s10973-020-09580-4

Muhammad, T., Waqas, H., Manzoor, U., Farooq, U., and Rizvi, Z. F. (2022). On doubly stratified bioconvective transport of Jeffrey nanofluid with gyrotactic motile microorganisms. *Alexandria Eng. J.* 61 (2), 1571–1583. doi:10.1016/j.aej.2021.06.059

Nazeer, M., Hussain, F., Khan, M. I., El-Zahar, E. R., Chu, Y. M., Malik, M. Y., et al. (2022). Theoretical study of MHD electro-osmotically flow of third-grade fluid in micro channel. *Appl. Math. Comput.* 420, 126868. doi:10.1016/j.amc.2021.126868

Poply, V. (2021). "Analysis of outer velocity and heat transfer of nanofluid past a stretching cylinder with heat generation and radiation," in *Proceedings of international conference on trends in computational and cognitive engineering* (Singapore: Springer), 215–234.

Rafiei, A., Loni, R., Mahadzir, S. B., Najafi, G., Sadeghzadeh, M., Mazlan, M., et al. (2022). Hybrid solar desalination system for generation electricity and freshwater with nanofluid application: Energy, exergy, and environmental aspects. *Sustain. Energy Technol. Assess.* 50, 101716. doi:10.1016/j.seta.2021.101716

Rashid, S., Abouelmagd, E. I., Khalid, A., Farooq, F. B., and Chu, Y. M. (2022). Some recent developments on dynamical h-discrete fractional type inequalities in the frame of nonsingular and nonlocal kernels. *Fractals* 30 (2), 2240110. doi:10.1142/s0218348x22401107

Rashid, S., Sultana, S., Karaca, Y., Khalid, A., and Chu, Y. M. (2022). Some further extensions considering discrete proportional fractional operators. *Fractals* 30 (01), 2240026. doi:10.1142/s0218348x22400266

Shruthy, M., and Mahanthesh, B. (2019). Rayleigh-bénard convection in casson and hybrid nanofluids: An analytical investigation. *J. nanofluids* 8 (1), 222–229. doi:10.1166/jon.2019.1571

Shuaib, M., Shah, R. A., and Bilal, M. (2020). Variable thickness flow over a rotating disk under the influence of variable magnetic field: An application to parametric bcontinuation method. *Adv. Mech. Eng.* 12 (6), 168781402093638. doi:10.1177/1687814020936385

Sun, T. C., DarAssi, M. H., Bilal, M., and Khan, M. A. (2022). The study of Darcy-Forchheimer hybrid nanofluid flow with the thermal slip and dissipation effect using parametric continuation approach over a rotating disk. *Waves Random Complex Media*, 1–14. doi:10.1080/17455030.2022.2072537

Syam Sundar, L., Sousa, A. C., and Singh, M. K. (2015). Heat transfer enhancement of low volume concentration of carbon nanotube-Fe3O4/water hybrid nanofluids in a tube with twisted tape inserts under turbulent flow. *J. Therm. Sci. Eng. Appl.* 7 (2), 021015. doi:10.1115/1.4029622

Ullah, I., Hayat, T., Alsaedi, A., and Asghar, S. (2019). Dissipative flow of hybrid nanoliquid (H2O-aluminum alloy nanoparticles) with thermal radiation. *Phys. Scr.* 94 (12), 125708. doi:10.1088/1402-4896/ab31d3

Ullah, I., Hayat, T., and Alsaedi, A. (2021a). Optimization of entropy production in flow of hybrid nanomaterials through Darcy–Forchheimer porous space. *J. Therm. Anal. Calorim.* 147, 5855–5864. doi:10.1007/s10973-021-10830-2

Ullah, I., Hayat, T., Aziz, A., and Alsaedi, A. (2022). Significance of entropy generation and the coriolis force on the three-dimensional non-Darcy flow of ethylene-glycol conveying carbon nanotubes (SWCNTs and MWCNTs). *J. Non-Equilibrium Thermodyn.* 47 (1), 61–75. doi:10.1515/jnet-2021-0012

Ullah, I., Ullah, R., Alqarni, M. S., Xia, W. F., and Muhammad, T. (2021b). Combined heat source and zero mass flux features on magnetized nanofluid flow by radial disk with the applications of Coriolis force and activation energy. *Int. Commun. Heat Mass Transf.* 126, 105416. doi:10.1016/j.icheatmasstransfer.2021.105416

Varun Kumar, R. S., Punith Gowda, R. J., Naveen Kumar, R., Radhika, M., and Prasannakumara, B. C. (2021). Two-phase flow of dusty fluid with suspended hybrid nanoparticles over a stretching cylinder with modified Fourier heat flux. *SN Appl. Sci.* 3 (3), 384–389. doi:10.1007/s42452-021-04364-3

Wang, F., Khan, M. N., Ahmad, I., Ahmad, H., Abu-Zinadah, H., and Chu, Y. M. (2022). Numerical solution of traveling waves in chemical kinetics: Time-fractional Fishers equations. *Fractals* 30 (2), 2240051–2240134. doi:10.1142/s0218348x22400515

Waqas, H., Manzoor, U., Muhammad, T., and Hussain, S. (2021). Thermo-bioconvection transport of nanofluid over an inclined stretching cylinder with Cattaneo–Christov double-diffusion. *Commun. Theor. Phys.* 73 (7), 075006. doi:10.1088/1572-9494/abfcb9

Zhang, M., Wang, X., and Øiseth, O. (2021). Torsional vibration of a circular cylinder with an attached splitter plate in laminar flow. *Ocean. Eng.* 236, 109514. doi:10.1016/j.oceaneng.2021.109514

Zhao, T. H., Khan, M. I., and Chu, Y. M. (2021). Artificial neural networking (ANN) analysis for heat and entropy generation in flow of non-Newtonian fluid between two rotating disks. *Math. Methods Appl. Sci.* doi:10.1002/mma.7310

Zhao, T. H., Wang, M. K., Hai, G. J., and Chu, Y. M. (2022). Landen inequalities for Gaussian hypergeometric function. *Rev. Real Acad. Ciencias Exactas, Físicas Nat. Ser. Matemáticas* 116 (1), 53–23. doi:10.1007/s13398-021-01197-y

Zhou, J. C., Abidi, A., Shi, Q. H., Khan, M. R., Rehman, A., Issakhov, A., et al. (2021). Unsteady radiative slip flow of MHD Casson fluid over a permeable stretched surface subject to a non-uniform heat source. *Case Stud. Therm. Eng.* 26, 101141. doi:10.1016/j.csite.2021.101141

Nomenclature

u, v Velocity components
α Curvature parameter
ϵ Curie temperature
M Magnetization
k Thermal conductivity $[Wm^{-1}K^{-1}]$
D_m Microorganism diffusivity
Ω Magnetic scalar potential
τ_{xy} Shear stress
β Casson fluid parameter
T_w Temperature at the surface
λ Viscous dissipation parameter
η Scaled boundary-layer coordinate
U_w Stretching velocity
K^* Pyromagnetic co-efficient
W_c Microbe floating speed
D_B Brownian motion
S_2 Concentration stratification
C_f Surface drag force
α_f Modified thermal diffusivity
P_e Bioconvection Peclet number
x, r Coordinate
T_w Temperature at wall
δ Bioconvection constant
H Magnetic field
C_p Specific heat
q_w Surface heat flux
μ_0 Magnetic permeability
w_1 Slip factor
μ Dynamic viscosity
T_∞ Ambient temperature $[K]$
ϕ_1 Volume fraction of nanoparticles
θ Dimensionless temperature
S_1 Thermal stratification
Pr Prandtl number
Re_x Rayleigh number
S_3 Microorganism stratification
s Velocity slip parameter
λ_c Concentration relaxation time
(ρC_p) Specific heat capacity
Nu_x Nusselt number